Charge Generation in PbS Quantum Dot Solar Cells Characterized by Temperature-Dependent Steady-State Photoluminescence

Jianbo Gao,[†,§] Jianbing Zhang,[†,‡,§] Jao van de Lagemaat,[†] Justin C. Johnson,[†] and Matthew C. Beard[*,†]

[†]Center for Advanced Solar Photophysics, National Renewable Energy Laboratory, Golden, Colorado 80401, United States and [‡]School of Optical and Electronic Information, Huazhong University of Science and Technology, 1037 Luoyu Road, Wuhan, People's Republic of China. [§]J. Gao and J. Zhang contributed equally to this work.

ABSTRACT Charge-carrier generation and transport within PbS quantum dot (QD) solar cells is investigated by measuring the temperature-dependent steady-state photoluminescence (PL) concurrently during *in situ* current–voltage characterization. We first compare the temperature-dependent PL quenching for PbS QD films where the PbS QDs retain their original oleate ligand to that of PbS QDs treated with 1,2-ethanedithiol (EDT), producing a conductive QD layer, either on top of glass or on a ZnO nanocrystal film. We then measure and analyze the temperature-dependent PL in a completed QD-PV architecture with the structure Al/MoO_3/EDT-PbS/ZnO/ITO/glass, collecting the PL and the current simultaneously. We find that at low temperatures excitons diffuse to the ZnO interface, where PL is quenched *via* interfacial charge transfer. At high temperatures, excitons dissociate in the bulk of the PbS QD film *via* phonon-assisted tunneling to nearby QDs, and that dissociation is in competition with the intrinsic radiative and nonradiative rates of the individual QDs. The activation energy for exciton dissociation in the QD-PV devices is found to be ~40 meV, which is considerably lower than that of the electrodeless samples, and suggests unique interactions between injected and photogenerated carriers in devices.

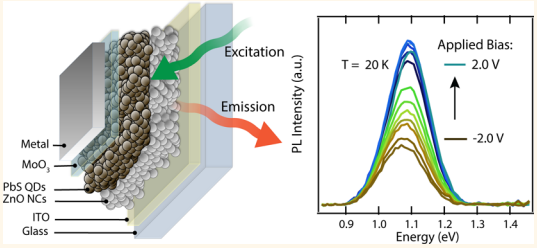

KEYWORDS: quantum dot · solar cell · photoluminescence · charge transport

Quantum dot (QD) thin films are an emerging class of tunable semiconductor layers with unique and beneficial characteristics that are being studied for optoelectronic applications, such as solar cells,[1−3] field-effect transistors,[4] light-emitting diodes,[5] and photodetectors.[6] For many optoelectronic applications that aim to utilize QDs there is a desire to maintain the beneficial properties inherent in the individual QDs while at the same time take advantage of the extended nature of the QD assembly. The field of QD films has seen rapid progress in the last 5 years as new procedures of QD film preparation have been developed that allow for increased QD–QD interactions resulting in larger charge-carrier mobilities. For example, electron mobilities in excess of 5 $cm^2\ V\ s^{-1}$ have been reported in the PbSe[7] and CdSe QD system,[8] while PbS QD-based photovoltaic (PV) cells have seen the power conversion efficiency rise from 2%[9,10] to near 9%[11,12] in just a few years. Improvements in device operation can result from better understanding as well as elucidating the factors that affect their operation. In particular, the nature of the photoexcited electron–hole pairs and the generation rate of free electrons and holes compared to the various recombination channels are important parameters that determine PV performance. In this study, we employ temperature-dependent photoluminescence (PL) quenching to study the charge generation within working QD solar cells. We find that the generation of mobile charge carriers is both temperature- and field-dependent. At room temperature the majority of excitons dissociate *via* phonon-assisted tunneling that quenches PL, while at low temperatures the photoexcited carriers remain as excitons and undergo radiative and nonradiative recombination.

* Address correspondence to matt.beard@nrel.gov.

Received for review October 24, 2014 and accepted December 8, 2014.

Published online December 08, 2014
10.1021/nn506075s

The applied voltage does increase the number of free charge carriers available for power generation, but its main role here is to sweep out the photogenerated carriers. Charge-separating interfaces can also dissociate excitons to produce free carriers but are more important at low temperature, where exciton dissociation within the bulk of the QD layer is suppressed.

RESULTS

Photoexcitation produces electron–hole pairs confined within individual QDs, or excitons. The confined excitons have in principle three generic decay channels: radiative and nonradiative recombination and electron–hole pair dissociation to form separated electrons and holes on separated QDs (Figure 1). The generation rate of mobile charge carriers in QD arrays is determined by a competition between exciton diffusion, with rate constant k_{ex}, exciton dissociation, with rate constant k_{diss}, and radiative, k_r, and nonradiative, k_{nr}, recombination on individual QDs. Once the electrons and holes are separated, they then need to reach their respective electrodes, where they can be collected in an external circuit prior to undergoing additional nonradiative and/or radiative recombination, but these recombination processes are secondary to the carrier generation process. Excitons are mobile,[13,14] and through diffusion they can occupy the lowest energy states[15] within the excitonic density of states of the QD ensemble under steady-state conditions. In this work, we monitor the exciton occupation through the PL intensity and PL peak energy as a function of temperature to study these competing processes.

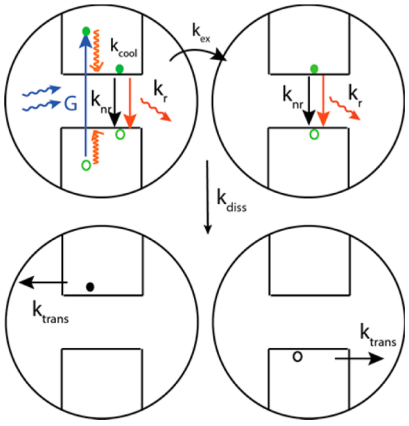

Figure 1. Light absorption occurs within individual QDs, and the photogenerated excitons (green circles) can undergo radiative or nonradiative recombination within the QD or diffuse to a nearby QD and then undergo exciton recombination. If the exciton dissociation energy is small enough, the excitons can dissociate to form free electrons (filled black circles) and holes (black circles) on separate QDs. These processes are in competition with one another. Once dissociated, the free carriers can drift or diffuse through the QD array and be collected within an external circuit.

Temperature-Dependent PL Quenching in Isolated PbS QD Films. We first restrict our analysis to the temperature-dependent PL of isolated PbS QD films that are not fully connected within a solar cell but were fabricated identically to the QD-PV devices discussed later. Figure 2 compares the temperature-dependent PL spectra for a PbS QD drop-cast film where the QDs retain their original oleic acid (OA) ligands (Figure 2a), a dip-coated PbS QD film where EDT is used to remove the oleate ligand and electronically couple the QDs (Figure 2b), and a 1,2-ethanedithiol (EDT)-treated PbS QD layer deposited on the top of a ZnO nanocrystal (NC) layer (Figure 2c) (layer stack typically used for solar cells). Figure 2d displays the shift in the PL position with temperature for each of the three films. In Figure 3a we plot the integrated PL intensity for these three cases as a function of temperature. The PL peak energy and

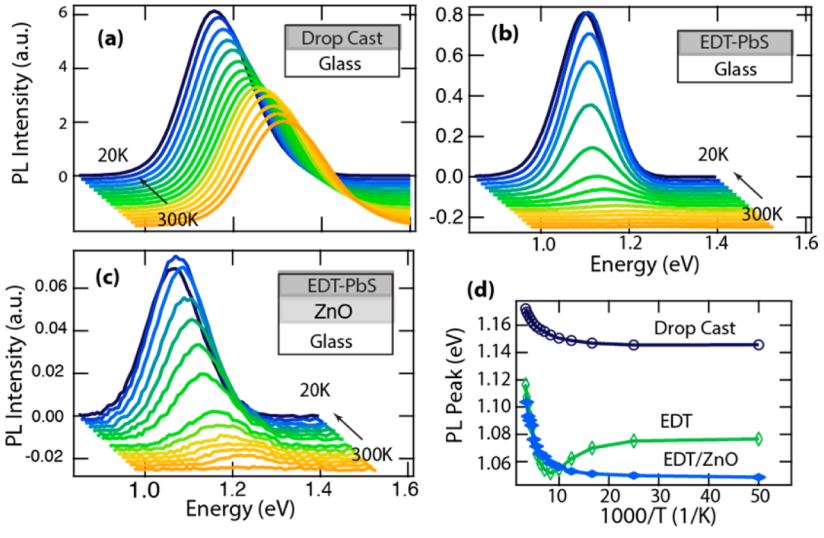

Figure 2. Temperature-dependent PL spectra from 20 to 300 K with a step of 20 K of (a) a drop-cast PbS QD film, (b) an EDT-treated PbS QD film, and (c) an EDT-treated PbS film on a ZnO NC layer. (d) PL peak energy as a function of temperature for each sample. Layer structures are shown in the inset.

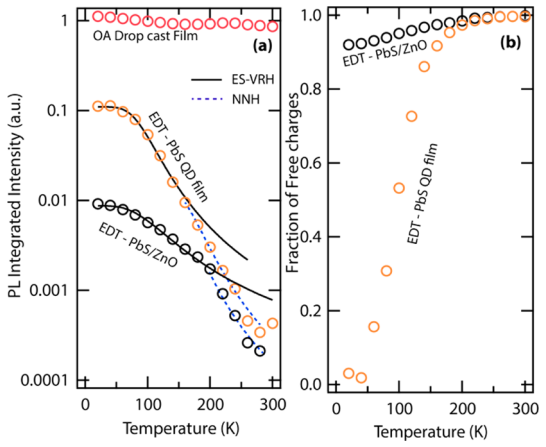

Figure 3. (a) Integrated PL intensity *vs* temperature for the oleate-terminated PbS QDs in either a drop-cast film (red circles), EDT-PbS QD film (orange circles), or EDT-PbS/ZnO film (black circles). The PL for each case was normalized to the PL quantum yield of the drop-cast film at $T = 18$ K. The black traces are for the Efros–Shklovskii variable range-hopping (ES-VRH) model, while the blue-dashed traces are for nearest neighbor hopping (NNH). (b) Fraction of free charges as a function of temperature for the two EDT-treated films (same symbols as in part a).

integrated PL intensity are extracted by fitting PL spectra with a Gaussian function. The relative PL intensities were normalized to the PL intensity of the drop-cast films at 18 K.

The temperature-dependent PL of insulated QDs (Figure 2a) behaves similarly to what has been previously reported,[16] while in the EDT-treated films the PL behavior changes drastically (Figure 2b) compared to the insulated QDs. First, there is an overall red-shift in the 1S energy level that is indicative of the increased electronic coupling (see Figure 2d comparing the peak energy of the drop-cast film to the EDT-treated film). Second, at 300 K the PL is nearly quenched in the EDT-treated films compared to the drop-cast films. The PL recovers at 18 K, but the emission is ~10× lower in the EDT-treated QD film (Figure 2b) compared to the film of oleate-capped QDs (compare Figure 3a, red *vs* orange traces). Third, the shift of the PL peak energy is also quite distinct in the treated films. Starting at 18 K, in the OA-terminated QD films there is an overall blue-shift of the PL with increasing temperature, while in the coupled film the PL first red-shifts and then blue-shifts, reaching a minimum around 80 K. The interplay between exciton diffusion within a bandtail density of states and temperature-dependent exciton dissociation can explain these observations.[17] In our model of the isolated QD films, PL arises only from excitons that have not undergone charge separation. The initial red-shift with increasing temperature, for the EDT-treated films, occurs because excitons in the high-energy part of the bandtail are preferentially thermally separated, leaving only those excitons that are deeper in the bandtail to emit at lower energies (see Figure 2d). Excitons equilibrate *via* a Förster resonance energy transfer (FRET) mechanism on time scales that are faster than radiative recombination,[15,18,19] thus leading to an overall temperature-independent red-shift since excitons can diffuse to larger QDs in the ensemble before they emit light.

Surprisingly, the PL characteristics are further modified when the same EDT-treated film is deposited on top of a ZnO NC film (Figure 2c and Figure 3a and b black trace). The PL intensity of the EDT-treated PbS QD film on top of ZnO decreases by a factor of ~10 at low temperatures compared with the QD film directly on glass. While the PL is still rapidly quenched with increasing temperatures, it is not quenched nearly as strongly as the EDT-treated film on glass. The PL peak only red-shifts with decreasing temperature and does not exhibit the blue-shift at the lowest temperatures. For temperatures less than 100 K, the peak PL energy from the EDT-PbS/ZnO is smaller than that of the isolated EDT-PbS (see Figure 2d comparing the EDT-PbS (blue trace) to EDT-PbS/ZnO film (green trace)). These differences can be attributed to the presence of the charge-separating interface introduced by the ZnO layer. The ZnO film is deposited prior to depositing the PbS QD layer and is therefore unlikely to affect the properties of the PbS QDs. ZnO and PbS form a bilayer rather than interdigitating, and the absorption depth is ~150 nm[20] (λ = 514 nm); thus, we estimate that less than ~1/10 of the PL could arise from QDs that are in direct contact with the ZnO interface and, thus, neglect reduction in PL due to potential interface states associated with the ZnO deposition or electron transfer from only those excitons that are directly produced nearest the ZnO layer. We conclude that at low temperatures excitons produced away from the interface diffuse to the ZnO interface and undergo charge separation. The interfacial charge transfer quenches the PL. Excitons within the higher energy portion of the bands diffuse faster[15] and are thus preferentially depopulated, while excitons that do not reach the interface are deeper in the bandtail and thus emit at lower energies. This explains why the PL peak energy for the PbS/ZnO stack remains at the position of the PbS-only layer and explains why the PL intensity is lower. For temperatures greater than ~200 K the PL behaviors of the EDT-PbS/ZnO and EDT-PbS films are nearly identical, implying that for temperatures greater than 200 K excitons produced within the EDT-PbS/ZnO film can no longer reach the ZnO interface prior to exciton dissociation within the bulk of the EDT-PbS film.

Temperature-Dependent Exciton Dissociation. We have verified that the integrated PL is linear in light intensity (Figure S1) under conditions of no applied field and thus neglect exciton–exciton interactions. We also restrict our analysis to reverse bias conditions where minority carriers are swept out of the device such that nonlinear recombination involving minority carriers is unlikely. In the picture we have outlined above light

emission occurs from radiative recombination of excitons and is in competition with exciton dissociation. The overall PL efficiency can be expressed as a product of the PL efficiency on an isolated QD (η'_{PL}) multiplied by the fraction of excitons that do not dissociate to form free carriers;[21] thus,

$$\eta_{PL}(T) = \eta_{PL}'(1 - \eta_{diss}(T)) = \frac{k_r}{k_r + k_{nr}}(1 - \eta_{diss}(T)) \quad (1)$$

where k_r and k_{nr} are the radiative and nonradiative rate constants of an exciton and η_{diss} is the efficiency of exciton dissociation. The fraction of free charges at a given temperature is then expressed by $\eta_{diss} = 1 - \eta_{PL}/\eta'_{PL}$; here we take η'_{PL} to be the value at 18 K and plot η_{diss} in Figure 3b for the EDT-PbS and EDT-PbS/ZnO films. As shown in Figure 3b, for temperatures greater than 200 K excitons dissociate to form free carriers for both films, and the fraction of free charge carriers is nearly 1. For temperatures less than 200 K the fraction of free carriers varies drastically between the two films. In particular, the fraction of free carriers decreases to nearly zero by 50 K for the EDT-PbS film, implying that exciton dissociation channels are nearly quenched at low temperatures, but the fraction of free carriers drops to only 0.85 for the EDT-PbS/ZnO films as excitons diffuse to the interface to generate free carriers.

The exciton dissociation is in competition with the radiative and nonradiative rates, and η_{diss} can be expressed as[21,22]

$$\eta_{diss}(T, F) = \frac{k_{diss}(T, F) + k_{diss}^{int}}{k_{diss}(T, F) + k_{diss}^{int} + k_r + k_{nr}} \quad (2)$$

where $k_{diss}(T, F)$ is the temperature- and field (F)-dependent exciton dissociation rate constant for exciton dissociation within the bulk of the PbS QD film, while k_{diss}^{int} is the exciton dissociation rate constant at the ZnO interface. k_{diss}^{int} contains both the rate of interfacial charge separation and the rate of exciton diffusion to that interface. We assume that the rate of exciton diffusion is the rate-limiting step, and thus, k_{diss}^{int} is determined by the exciton diffusion rate. Comparing the temperature-dependent PL of the uncoupled PbS QDs (red circles in Figure 3a) to the coupled PbS QD films (orange and black circles), we conclude that the PL quenching is dominated by the temperature-dependent k_{diss} rather than temperature-dependent radiative and/or nonradiative recombination. While the nonradiative rate increases in coupled films because the excitons can diffuse to more defective QDs,[14] recent studies suggest that exciton diffusion either is not temperature-dependent[23] or depends weakly on temperature.[15] Thus, in the following analysis we do not consider the radiative, nonradiative, and exciton diffusion rates to be temperature-dependent, and for this reason only k_{diss} must be temperature-dependent in eq 2.

The temperature-dependent exciton dissociation, or charge transfer between two QDs, has been found to follow phonon-assisted tunneling,[18,24] and the most general form of the dissociation rate constant (at $F = 0$) is given by[25]

$$k_{diss}(T; 0) = A \exp(-(\gamma/T)^{\nu}) \quad (3)$$

where γ is a characteristic temperature, A is a preexponential factor involving the attempt frequency of QD−QD charge tunneling events and ν is an exponent that describes the low-temperature hopping conductivity behavior of disordered systems.[26] If $\nu = 1$, then we recover nearest neighbor hopping (NNH) behavior and $\gamma = E_a/k_B$, where E_a is the activation energy and k_B is the Boltzmann constant. If $\nu = 0.5$, then we recover the Efros−Shklovskii variable range hopping (ES-VRH)[26] model, and if $\nu = 0.25$, the Mott VRH model in three-dimensional systems is found with $\gamma = T^*$. We find that no single value of ν can adequately describe the data across the entire temperature regime, as shown in Figure 3a. At low temperatures a value of 0.5 (thin black trace) describes the data best, while at higher temperatures $\nu = 1$ (thin blue trace) is better. A further discussion of the applicability of VRH can be found in the Supporting Information. There is a characteristic crossover temperature, T_c, where the behavior changes from $\nu = 1$ to 0.5. The activation energy E_a, T^*, and T_c are related by the following: $E_a = k_B(T^*T_c)^{1/2}$. Therefore, we modeled our data using one fitting function based on eqs 2 and 3 that switches from $\nu = 1$ to $\nu = 0.5$ at the crossover temperature. In the modeling, E_a, T_c, and A are varied across the full temperature range, and T^* is then calculated from the relationship described above. The EDT-PbS film was modeled by setting k_{diss}^{int} to be zero, and we find that E_a is 93(5) meV with a crossover temperature of 146 K. To model the EDT-PbS/ZnO films, we first held all parameters constant at the values determined from modeling the EDT-PbS film and only introduced a nonzero value of k_{diss}^{int} to recover the measured data. We find that just by introducing k_{diss}^{int} we can account for ∼90% of the differences between the quenching behavior of the two films. However, it is clear from our data that the crossover temperature increases in the EDT-PbS/ZnO film, and we find the best fit occurs when E_a decreases to 85(5) meV and the crossover temperature increases to 180 K.

The crossover temperature, T_c, changes from 146 K for the EDT-PbS film to ∼180 K for the EDT-PbS/ZnO films. According to Liu *et al.* the crossover temperature is related to when the optimized hopping distance is on the order of the nearest neighbor distance.[27] A higher crossover temperature implies that the distance a carrier must tunnel to find a QD with a similar energy level is larger. Such a scenario occurs when the excitons are deeper in the bandtail and are thus less likely to be near a QD with the appropriately aligned energy level.

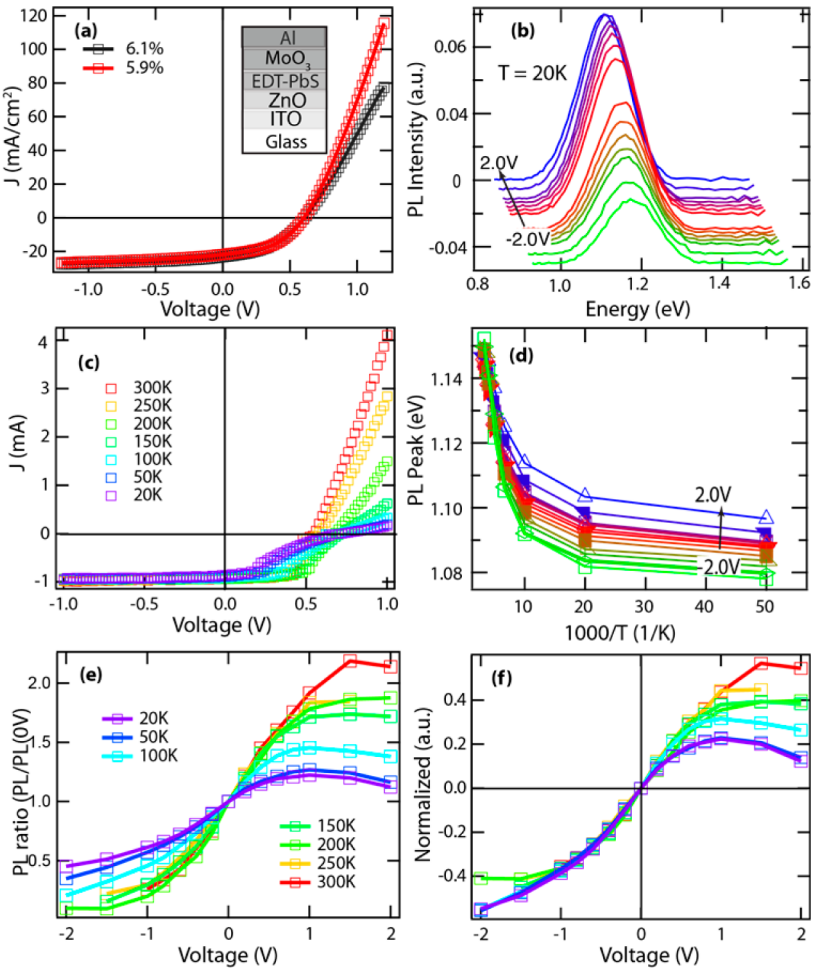

Figure 4. (a) Device current density−voltage characteristics using 1-Sun solar light intensity illumination. The device structure is shown in the inset. (b) PL spectra as a function of bias for the 6.1% device at a temperature of 20 K. PL was collected at −2, −1.5, −1, −0.8, −0.6, −0.4, −0.2, 0.2, 0.4, 0.6, 0.8, 1, 1.5, and 2 V. (c) Current density−voltage characteristics of the device as a function of temperature collected under identical conditions to the PL data in part (b). (d) Peak PL energy as a function of temperature various applied biases. (e) Integrated PL as a function of applied bias for the various temperatures. The PL intensity for each temperature is normalized by the PL intensity at open circuit (0 V). (f) The same as part (e), but the PL for each temperature is normalized between −1 and 0 V.

This observation is consistent with the lower peak PL energy in the EDT-PbS/ZnO films, where excitons that are higher in the bandtail undergo dissociation at the ZnO interface, leaving only excitons deeper in the bandtail. The lower activation energy could be associated with a field that builds up under steady-state conditions due to the charge separation across the ZnO/PbS interface.

PL Quenching in Device-Structured PbS QD Films. We next investigated the temperature-dependent PL in devices made from the same EDT-treated PbS QDs. In Figure 4a we show the *I*−*V* characteristics at 1-Sun light intensity illumination of two devices studied here with power conversion efficiencies of 5.9% and 6.1%. A schematic of the device stack is shown in the inset of Figure 4a. All measurements discussed here were performed on both device structures, and the results were consistent. Since there are no major differences, we present results only from the 6.1% device. In Figure 4b we display typical PL spectra for a device at 20 K at various applied biases ranging from −2 to 2 V. We also recorded PL spectra at temperatures of 50, 100, 150, 200, 250, and 300 K. Figure 4c displays the current collected concurrently with the PL for the various temperatures. Figure 4d shows how the peak PL changes with temperature for applied biases. In Figure 4e we show the integrated PL for a series of bias values normalized to the integrated PL at open-circuit conditions as a function of temperature. Figure 4f displays the integrated PL normalized so that the values in the range of 0 to −1 V overlap.

We have the following observations from Figure 4a−f: (1) The PL characteristics including PL quenching and peak energy shifting of the EDT-PbS film within a device stack are similar (at zero applied bias) to those of the EDT-PbS/ZnO film shown in Figure 2c, while in general the PL intensity follows the *IV* characteristics for reverse and forward bias conditions. (2) Under reverse bias where current is extracted, the PL is further quenched. (3) In contrast,

the PL intensity is enhanced with increasing forward bias until it saturates at ~1.0 V and then is quenched with increasing forward bias, while the current continues to rise. Similar PL intensity dependence with reverse and forward bias also was reported in other thin-film solar cells.[28−30] The increase in PL at modest forward bias likely results from electrons and holes accumulating at the PbS/ZnO interface that enhances radiative recombination of separated electrons and holes, which does not occur in the unconnected QD films. However, further increase of the electrical field above 1.0 V induces additional nonradiative recombination channels such as Auger recombination due to the large injected carrier density. In forward bias, the injected carrier density can exceed the photogenerated carrier density, such that the photogenerated carriers have an increased likelihood of encountering a charged QD and undergoing nonradiative Auger recombination, while the current is not significantly affected at room temperature.

In reverse bias the PL quenching *vs* bias curves can be overlaid on top of one another (Figure 4f), indicating that where current is extracted the PL is quenched. Such behavior is supportive of the model described here, where exciton dissociation is limited by exciton recombination. A similar observation was made by Leatherdale *et al*. for films of CdSe QDs.[22] In that study, as here, they found that PL is quenched where photocurrent is collected. However, at 0 V bias the temperature-dependent PL quenching behavior is opposite of what is observed here. With decreasing temperature the PL is quenched, while here the PL quenches with increasing temperature. They concluded that the nonradiative and radiative processes on individual QDs determine the temperature-dependent PL intensity and that thermal dissociation of excitons was negligible. This is a similar situation to the uncoupled OA-terminated PbS QDs, where the temperature-dependent PL is indicative of the intrinsic properties of the QDs and not affected by the QD−QD interactions within the QD assembly. Upon application of a field, the PL is quenched and the photocurrent enhanced *via* exciton dissociation. In that study, the QD−QD separation was much larger than in our study; therefore the energy required to separate excitons was larger than the available thermal energy, and application of a field was necessary to overcome the energy barriers between the QDs and ionize the excitons. However, in our case the QDs are closer and dielectric constant higher, and this facilitates exciton dissociation; the exciton dissociation dominates the PL quenching behavior rather than the intrinsic radiative and nonradiative process of the individual QDs, and the field is not needed to ionize the QDs.

In contrast to the reverse bias conditions, the PL quenching curves deviate from one another under forward bias conditions (see Figure 4e and f), where Auger recombination events can occur with a higher probability. The deviation occurs at lower forward bias conditions for lower temperatures. At lower temperatures, excitons do not dissociate within the bulk of the film but rather can diffuse, and some fraction will reach the ZnO/PbS interface, where, under forward bias conditions, electrons are injected into the PbS film, rather than being extracted, and therefore cause nonradiative Auger recombination. However, at higher temperatures, exciton dissociation occurs prior to exciton diffusion, and therefore the likelihood of Auger recombination is reduced. Such behavior likely also causes the poor *IV* characteristics at lower temperatures (Figure 4c).

In order to further demonstrate the effect of temperature and electric field on PL and photocurrent in our solar cells, we first compare the temperature-dependent photocurrent (Figure 5a, solid traces) and PL intensity (Figure 5a, dashed traces) for conditions of reverse bias (blue traces) and forward bias (red traces). The photocurrent under reverse bias conditions does not change significantly with temperature, because at higher temperatures charges are generated *via* thermal dissociation of carriers. However, at low temperatures, carriers are generated by those excitons that diffuse to the ZnO interface. In both cases the field acts to sweep out the carriers. In forward bias conditions the field increases the current and reduces the PL. Excitons that reach the ZnO/PbS interface cause a reduction in PL due to increased Auger recombination and reduction in the current. The PL spectra peak position as a function of bias for various temperatures is shown in Figure 5b. Under reverse bias condition and at low temperature, excitons can be dissociated at the ZnO interface, but the charge separation can be assisted by the applied field. Under higher reverse bias the remaining excitons (those that emit light) populate states deeper in the band, inducing a further red-shift in the PL. Thus, at 20 K the PL emission energy further red-shifts by ~25 meV between +2 V and −2 V bias. At high temperatures excitons dissociate *via* thermal activation, and the electric field is less important to carrier generation and thus does not greatly affect the position of the PL. Thus, we conclude that at room temperature the field mainly sweeps carriers out of the device rather than dissociating excitons.

We plot the PL intensity as a function of temperature for various biases in Figure 6a. The dashed black trace in Figure 6a indicates the crossover temperature where the behavior changes from ES-VRH to NNH. We modeled the data in the same fashion described for the temperature-dependent PL for the EDT-PbS and EDT-PbS/ZnO films (Figure 2a). In this case, we find that T^* is nearly constant for all biases and E_a varies approximately linearly with the applied field, for biases ranging from −1 to 1 V (dashed green trace). The extracted activation energy and crossover temperature T_c are plotted in Figure 6b. The activation energy varies

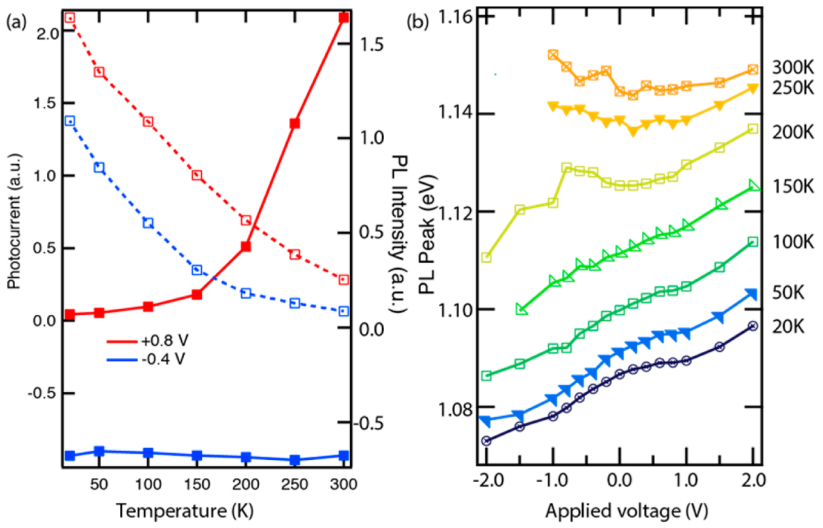

Figure 5. (a) Comparison of the temperature-dependent photocurrent (solid lines and solid squares) for forward bias (red traces) and reverse bias (blue traces) conditions and temperature-dependent PL intensity (dashed lines and open squares) for forward bias (red trace) and reverse bias (blue trace). (b) PL peak energy as a function of bias voltage at various temperatures. At reverse bias, the electrical field assists electron and hole flow to contribute to the photocurrent extracted by the electrodes, resulting in PL intensity quenching.

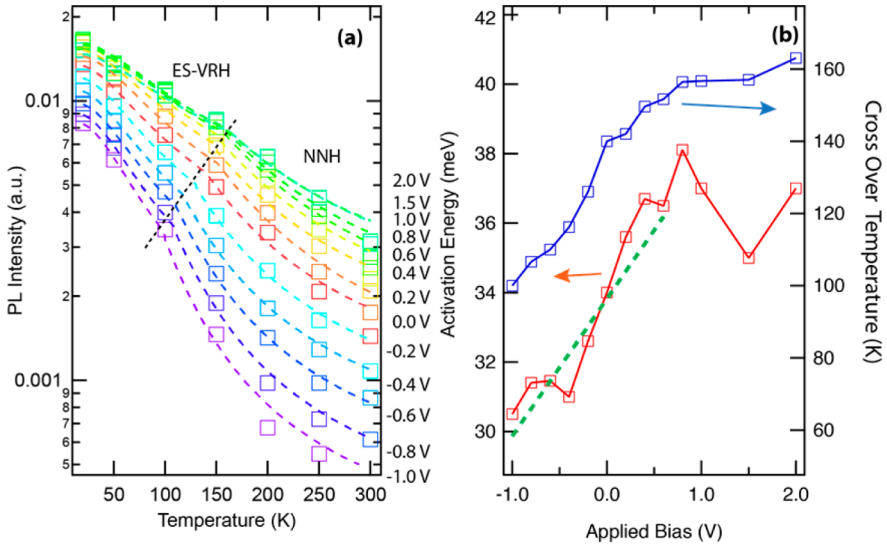

Figure 6. (a) Integrated PL intensity as a function of temperature for a variety of applied biases (indicated on the right side). The dashed curves are fits to the data using the NNH and ES-VRH models discussed in the text. The dashed black line represents the crossover from VRH to NNH. (b) Extracted values of the crossover temperature (blue squares) and the activation energy (red squares). The green dashed line is a linear dependence of the activation energy on applied bias.

approximately linearly from 30 to ~38 meV when the bias is changed from −1 to ~1 V. For forward bias greater than ~0.6 V the activation energy saturates. An applied voltage of ~0.6 V is close to flat band conditions. Such an applied voltage counteracts the photovoltage, producing zero net current in the circuit. In this regime the field mainly acts on the electrically injected carriers that dominate over the photogenerated carriers.

DISCUSSION

Photoluminescence *vs* Conductivity Measurements. The PL data presented here differ in several key features compared to temperature-dependent dark conductivity measurements of QD solids: (1) PL quenching is most sensitive to exciton dissociation that occurs at QD−QD interfaces rather than electron or hole hopping conductivity that occurs over a large set of QDs; (2) PL measurements necessarily involve the optical generation of electrons and holes on individual QDs, whereas in dark conductivity measurements electrons and/or holes are injected into the conduction or valence band *via* an external source. Equation 3 is a valid description of exciton dissociation and has a similar form to that describing electron/hole hopping conductivity,[27] but the physics are not necessarily

equivalent. The derivation of eq 3 arises by considering the tunneling probability of a charge between two sites separated by a distance r and depends upon the energy difference between the two sites and the hopping distance relative to the localization length. In conductivity measurements the transport is assumed to be limited by the tunneling probability of charges between two QDs within the array, and thus eq 3 is also used to describe conductivity. The key difference being in the conductivity case, charge carriers hop from a charged QD to a neutral QD, while for exciton dissociation discussed here the initial state is neutral and the final state consists of two QDs that are oppositely charged.[22]

Recently we studied the PL quenching behavior for a series of ligand treatments for both PbS and PbSe QD films. We studied how the PL quenching temperature (the temperature at which the PL is reduced to 50% of its peak value) varies as a function of the ligand length used for QD film formation.[24] The ligand length sets the average QD−QD distance and thus defines the QD−QD electronic tunneling rate.[31] We found a strong correlation between the ligand-length-dependent mobility measured in FET measurements with the PL quenching temperature. In particular, we found that by analyzing the pre-exponential factor (A in eq 3), values of β, the parameter that describes wave function leakage, could be extracted and resulted in values that were similar to those obtained from FET measurements. Those studies support our conclusion that eq 3 describes similar physics to charge hopping. Complications and thus differences between PL and conductivity would arise if, in fact (contrary to our assumption in eq 2), the radiative and/or nonradiative rates on individual QDs were strongly temperature-dependent, a situation we neglect here since our measurements of insulated QDs indicate weakly temperature-dependent behavior.

For QD films with longer ligands the QD films emit light at low temperatures with PL quantum yields (PLQY) similar to that found for QDs in solution and OA-capped films (20−40%), suggesting, as we have argued here, that at low temperatures excitons remain localized on the QDs. For that study and here, we find the PL remains largely quenched at 18 K for EDT-treated films, suggesting that significant charge generation and/or another PL quenching mechanism occurs at 18 K for the EDT-treated films that is not present for the oleic acid-terminated QDs. There are three possible scenarios that could explain these observations. (1) At 18 K there is enough thermal energy to dissociate excitons; (2) the EDT treatment increases the nonradiative rates on individual QDs, leading to an overall lower PL; and (3) an increased exciton diffusion rate allows for excitons to find defective QDs and undergo nonradiative recombination. We can rule out possibility 1 because the PL quenching behavior

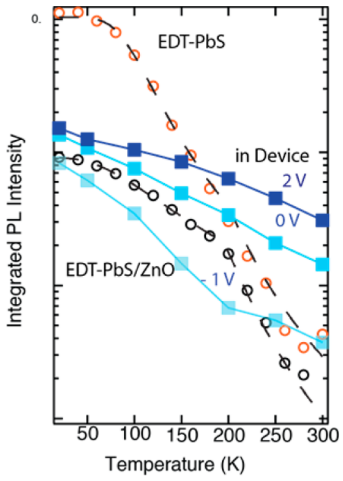

Figure 7. PL quenching from Figure 2 a for the EDT-PbS (red circles) and EDT-PbS/ZnO films (black circles) compared directly with the PL quenching within the QD-PV device for 2, 0, and −1 V applied bias in blue-shaded squares (data are taken from Figure 5a).

is already beginning to saturate at 18 K, indicating that there is insufficient thermal energy to dissociate excitons. Therefore, we conclude that reduction of the PL at 18 K is likely related to a combination of increased defect density due to the EDT treatment and increased exciton diffusion rate. The exciton diffusion rate scales as $1/R^6$ where R is the center-to-center distance between acceptor and donor QDs, and thus exciton diffusion is faster for the EDT-treated films relative to the OA-terminated QDs. Wagner *et al*. measured the trapped charge density for a series of PbS QD films that were treated with various chemical treatments typically used for PbS QD PV device fabrication.[14] While they did not study an EDT-treated film, they did study a benzenedithiol (BDT)-treated film and found that the defect density was fairly high for the BDT-treated film compared to other treatments, which supports our conclusion here that the EDT treatment introduces a larger fraction of defects that can quench PL.

PL in Isolated QD Layers *vs* PL from QD Layers Incorporated into PV Structures. Surprisingly, the PL quenching behavior is quite different in the QD layer incorporated into the PV architecture compared to the EDT-PbS and EDT-PbS/ZnO films. Figure 7 shows a direct comparison of the PL quenching from the PV film and from the non-PV films. There are two interesting observations that can be made: (1) The activation energy is at least 2 times smaller even under flat band conditions in the PV film, which can easily be seen from the smaller slope of the PL quenching at 0 and 2 V, despite the fact that in reverse bias (−1 V) the PL quenching is similar to that of the EDT-PbS/ZnO film; (2) the PL is not 100% quenched in reverse bias at room temperature and is in fact *higher* than that of the EDT-PbS QD layer, indicating that the PL is *less* quenched. The major fabrication difference is that of the Al and MoO_3 deposition steps. During these

steps the QD layer is first subjected to high-vacuum conditions and then followed by the actual deposition. To test whether this could be responsible for our observations, we prepared an EDT-PbS layer on glass and then deposited MoO_3 and Al on the back side of the substrate rather than the QD-layer side. We observed similar PL behavior to the EDT-PbS QD films discussed here, which eliminates the vacuum conditions as a contributor to the observed differences. It is possible that the metal deposition on top of the QD layer causes the film to undergo slight annealing. However, we disregard this situation because we have not observed other features associated with annealing of QD layers. For example, the optical absorption remains the same in the device *vs* nondevice architectures. Finally, it is possible that MoO_3 and or Al could diffuse into the QD layer and passivate surface states. Choi *et al*. found that in CdSe FET devices indium could diffuse and passivate midgap states in the CdSe QDs. Filling the midgap states resulted in improved carrier transport.[8] Such a process could occur in our films with Al rather than indium.

A more likely scenario than those based on how the QDs were treated during film or device formation is that the lower activation energy and higher PL at room temperature are associated with PL that can arise from a dissociated electron or hole that then recombines with an injected electron or hole. Under reverse bias conditions, only photocurrent flows in the device, and the applied field acts only to sweep out charges rather than injecting carriers, while at flat band conditions carriers are injected to flatten the bands. Thus, the density of injected carriers increases for increased forward bias and thus increases the likelihood that photogenerated carriers will undergo radiative emission. Finally another scenario is that the lower activation energy could also arise due to screening of charges that lowers the Coulomb binding energy of the excitons. More work is needed in order to fully understand these observations.

Transport and PL within Bandtails. In previous studies, we employed steady-state temperature-dependent PL to characterize the behavior of photogenerated carriers within QD films. The results could be described by assuming an exponentially decaying bandtail of excitonic states that extends below a mobility edge. The falloff of density of states, referred to typically as the Urbach energy, depends on QD size, ligand length, and ligand chemical identity.[17] In addition to observing behavior consistent with bandtail states in the temperature-dependent PL we also observed similar bandtail behavior in the electrical conduction of the QD optoelectronic devices,[32] suggesting that the density of excitonic states and the density of electronic states are similar. These similarities suggest that the conductivity of carriers is mainly governed by hopping between quantized levels of the QDs and not associated

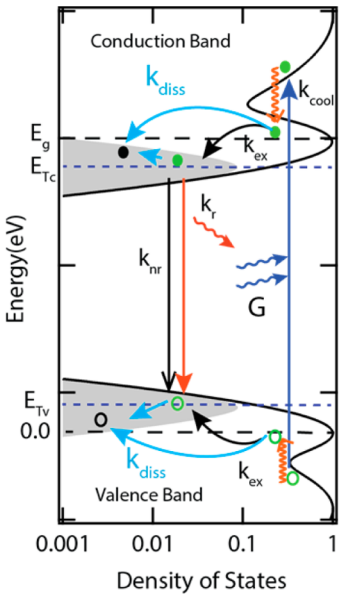

Figure 8. Bandtails associated with excitonic and electronic states. Excitons are produced within the QDs and quickly thermalize to the bottom of the Gaussian distribution of states (denoted by shaded region). Exciton dissociation occurs from the bottom of the DOS *via* thermally assisted tunneling.

with a shallow surface-related defect level. It is possible that such shallow defect levels could have a density of states similar to that of the excitonic density of states, but we think such a coincidence is unlikely. The tail of a Gaussian distribution can be approximated with an exponential function and could, therefore, define the Urbach energy measured in the two experiments. Thus, in our picture transport occurs *via* thermally assisted hopping within the largest subset of QDs within the ensemble.

A simple picture of how the QD photophysics proceeds within an array of electronically coupled QDs is shown in Figure 8. Excitons are produced *via* absorption of light within the individual QDs and partitioned according to the optical absorption of the QD ensemble. The as-produced excitons undergo a competition between exciton diffusion, exciton dissociation, and nonradiative and radiative recombination. During exciton diffusion, any defective QDs within the ensemble could quench the PL, resulting in a reduced PL compared to isolated QDs where a small subset of defective QDs are statistically less likely to be photoexcited. The excitons and/or carriers then occupy the tail of the DOS (pictured here as the shaded region) whose distribution is defined on the low-energy side by the tail of the DOS and on the high-energy side by the system temperature. A quasi-Fermi energy defines the transport edge for electrons and holes and is denoted by E_{Tc} and E_{Tv}. If a charge-separating interface is in contact with the QDs, the excitons can diffuse to the interface. However, at room temperature the excitons are dissociated prior to significant exciton

diffusion. The applied bias sweeps carriers out of the device. In the work of Wagner *et al.*, they concluded that exciton diffusion to defective QDs was a major limiting process for PbS QD devices.[14] However, mid-gap states that trap carriers also play a role in limiting device operation because otherwise separated carriers could undergo nongeminate radiative recombination and the PL efficiency would not be quenched at room temperature.

Mentzel and co-workers studied dark transport in annealed PbSe QD films measured in an FET device and found a transport activation energy of ~40 meV,[33] which is coincidentally the same as found here. They also note that the activation energy for hole transport is consistently smaller than the site energy dispersion caused by variations in the size of the QDs and concluded that the Fermi energy was in the tail of the $1S_h$ band and is defined by a surface donor state. The differences between this study and the Mentzel study are that here we are studying EDT-treated PbS QDs rather than annealed PbSe QDs films, and we have measured the activation energy for charge generation from an electron−hole pair generated by light. Here, in our study, the activation energy is also smaller than the site energy dispersion, which can be estimated from the absorption spectra to be ~80−100 meV. In our previous PL quenching study, in which ligand treatments and QD size were varied, no correlation was observed between the size dispersion and activation energy. Since the excitons can thermalize within the bandtail and carrier transport also occurs within the bandtail, the activation energy can be smaller than the size distribution. However, a narrower size distribution should allow for a smaller difference between the exciton band gap and the transport edge and thus improve the device performance.

Field-Dependent Effects. Application of a field lowers the activation energy,[33] making it more likely for excitons to tunnel between adjacent QDs; therefore, the crossover to the NNH regime occurs at a lower temperature. According to the model proposed by Mentzel *et al.*, the change in the activation energy is $E_a \rightarrow E_a - eFx$, where x is the distance the carriers move upon dissociation, and thus, $\Delta E_a = -eFx$. In the case of a photovoltaic device the field is not uniformly dropped across the entire device stack, as in the case of an FET device, because each layer in the device has a different resistance. In our studies, we estimate that ~50% of the field is dropped across the ZnO layer, with some fraction dropping across the MoO_3 layer as well. Therefore, we estimate that ~10−20% of the field is dropped across the photoactive region of the PbS QD layer. In Figure S3 we plot the field (assuming 15% of the applied field is dropped across the PbS layer) *vs* the activation energy. A best-fit line has a slope that yields a charge separation distance of $x = 5.5 \pm 0.5$ nm, which is about twice the diameter of the QDs used here, ~2.8 nm. However, given our uncertainties in calculating the field across the PbS layer, this is in reasonable agreement with the notion that exciton dissociation occurs *via* tunneling from/to the localized 1S states of the QDs.

CONCLUSIONS

We monitored both the shift of the peak PL energy and the intensity of PL as a function of temperature in isolated QD films and in QD films that are incorporated into ~6% QD-PV architectures. The behavior of excitons in the QD films depends significantly on the temperature. At low temperatures excitons are the dominant species and can diffuse over 100's of nanometers. When a charge separation interface is present, the PL is further quenched by excitons that diffuse to that interface. Excitons, therefore, sample and can be quenched by a small subset of defective QDs. Defect states that can quench excitons are important to consider, but defects that trap free carriers are also important in the operation of the QD PV devices. At low temperatures excitons equilibrate into the lowest energy part of the QD ensemble. At higher temperatures excitons dissociate to form free charge carriers before reaching a junction. The activation energy for exciton dissociation in QD-PV films is ~40 meV, similar to activation energies measured in dark conductivity measurements, indicating that the physics for charge separation and charge transport are similar. Narrowing the size-distribution of the QD ensemble should allow for improved device performance by narrowing the bandtails and moving the transport edge closer to the center of the distribution. The role of the applied bias is mainly to sweep out the charge carriers rather than dissociate excitons. Temperature-dependent steady-state photoluminescence can provide valuable information about the complex exciton and carrier dynamics in QD solids. Ideally, the PL should not quench at higher temperatures, but instead the PL mechanism would change from excitonic recombination at low temperatures to carrier radiative recombination above the temperature threshold for exciton dissociation.

EXPERIMENTAL SECTION

Nanocrystal Synthesis. Synthesis of ZnO NCs was carried out following previous literature reports[34,35] by adding 4.4 g of ZnAc to 200 mL of methanol, heating to 60 °C with a dropwise addition of 100 mL of a 0.4 M KOH solution in methanol. The solution was stirred at 60 °C for 2 h. The particles were extracted *via* centrifugation and resuspension in methanol. This was repeated three times, and finally the dry ZnO powder was dispersed in 40 mL of chloroform. We synthesized PbS QDs with a first exciton peak at 920 nm (1.34 eV) by adding 1.8 g of PbO, 8.25 g of oleic acid, and 14 g of 1-octadecene to a

three-neck round-bottom flask. This mixture was heated to 120 °C under vacuum for 2 h and then placed under N_2. In a glovebox, 180 μL of hexamethyldisilathiane was mixed with 5 mL of octadecene and loaded into a syringe. The contents of the syringe were injected into the flask, and the heating mantle was immediately removed while the QDs were cooled to room temperature. The reaction solution was mixed with 10 mL of hexane and 20 mL of ethanol and centrifuged to extract the QDs. Hexane and ethanol were used again for an additional purification step, and the oleate-capped QDs were then suspended in hexane and stored in air or a N_2 desiccator until use.

Device Fabrication. Nanocrystalline ZnO was spin-coated on patterned ITO glass slides (Thin Film Devices, Anaheim, CA, USA) with an active device area of 0.11 cm^2 and then heated on a hot plate in air at 260 °C for 30 min. The PbS QD layer (3.5 nm diameter QDs) was deposited as described before. In particular, QD layers were deposited onto the ZnO layer *via* sequentially immersing the substrate into a suspension of PbS QDs in hexane (10 mg/mL solution) followed by a 1 mM 1,2-ethanedithiol solution in acetonitrile. This process was repeated until the thickness of the QD film reached ~364 nm. For annealing, the PbS QD thin films were transferred to a hot plate in a glovebox set to a temperatures of 100 °C for 30 min. The PbS film was then loaded from ambient air into the evaporation chamber, where a 10−15 nm thick MoO_x film was thermally evaporated at a rate of 0.5 Å/s under a base pressure of ~10^{-6} Torr, and a 100 nm Al top contact was then thermally evaporated at a base pressure of 10^{-7} Torr without breaking the vacuum.

Steady-State PL. Temperature-dependent PL spectra were conducted under vacuum (<10^{-5} Torr) in a closed-loop He cryostat. Bare films on glass substrates or device films were excited with 47 mW Ar-ion laser excitation at 514 nm. The excitation beam was unfocused (spot size roughly 3 mm diameter) and mechanically chopped at 1 kHz. The laser illuminates through glass substrates, and the resulting PL spectra were collected at the same side and detected with an amplified Ge photodiode routed to a lock-in amplifier. Spectra were corrected for monochromator and detector efficiencies using a calibrated lamp. For each sample, spectra were always collected beginning at the lowest temperature and warming to the highest. Samples were left stationary in the cryostat during measurement of an entire temperature range. No rapid photobleaching or degradation effects were observed during PL measurements. At powers of <50 mW, successive, repeated measurements at the same temperature produced identical emission spectra.

Conflict of Interest: The authors declare no competing financial interest.

Supporting Information Available: Experimental details, PL laser fluence dependence, discussion and presentation of VRH *vs* NNH model, and activation energy *vs* applied field. This material is available free of charge *via* the Internet at http://pubs.acs.org.

Acknowledgment. We acknowledge helpful discussions with Joseph Luther and Rachelle Ihly. The material presented here is based upon work supported by the U.S. Department of Energy Office of Science, Office of Basic Energy Sciences Energy Frontier Research Centers program within the Center for Advanced Solar Photophysics. DOE funding was provided to NREL through contract DE-AC36-08GO28308.

REFERENCES AND NOTES

1. Semonin, O. E.; Luther, J. M.; Choi, S.; Chen, H. Y.; Gao, J. B.; Nozik, A. J.; Beard, M. C. Peak External Photocurrent Quantum Efficiency Exceeding 100% *via* MEG in a Quantum Dot Solar Cell. *Science* **2011**, *334*, 1530–1533.
2. Gao, J. B.; Perkins, C. L.; Luther, J. M.; Hanna, M. C.; Chen, H. Y.; Semonin, O. E.; Nozik, A. J.; Ellingson, R. J.; Beard, M. C. n-Type Transition Metal Oxide as a Hole Extraction Layer in PbS Quantum Dot Solar Cells. *Nano Lett.* **2011**, *11*, 3263–3266.
3. Sargent, E. H. Infrared Photovoltaics Made by Solution Processing. *Nat. Photonics* **2009**, *3*, 325–331.
4. Liu, Y.; Gibbs, M.; Perkins, C. L.; Tolentino, J.; Zarghami, M. H.; Bustamante, J.; Law, M. Robust, Functional Nanocrystal Solids by Infilling with Atomic Layer Deposition. *Nano Lett.* **2011**, *11*, 5349–5355.
5. Sun, L. F.; Choi, J. J.; Stachnik, D.; Bartnik, A. C.; Hyun, B. R.; Malliaras, G. G.; Hanrath, T.; Wise, F. W. Bright Infrared Quantum-Dot Light-Emitting Diodes through Inter-Dot Spacing Control. *Nat. Nanotechnol.* **2012**, *7*, 369–373.
6. Guo, F. W.; Yang, B.; Yuan, Y. B.; Xiao, Z. G.; Dong, Q. F.; Bi, Y.; Huang, J. S. A Nanocomposite Ultraviolet Photodetector Based on Interfacial Trap-Controlled Charge Injection. *Nat. Nanotechnol.* **2012**, *7*, 798–802.
7. Liu, Y.; Tolentino, J.; Gibbs, M.; Ihly, R.; Perkins, C. L.; Liu, Y.; Crawford, N.; Hemminger, J. C.; Law, M. PbSe Quantum Dot Field-Effect Transistors with Air-Stable Electron Mobilities above 7 cm^2 V^{-1} s^{-1}. *Nano Lett.* **2013**, *13*, 1578–1587.
8. Choi, J. H.; Fafarman, A. T.; Oh, S. J.; Ko, D. K.; Kim, D. K.; Diroll, B. T.; Muramoto, S.; Gillen, J. G.; Murray, C. B.; Kagan, C. R. Bandlike Transport in Strongly Coupled and Doped Quantum Dot Solids: A Route to High-Performance Thin-Film Electronics. *Nano Lett.* **2012**, *12*, 2631–2638.
9. Luther, J. M.; Law, M.; Beard, M. C.; Song, Q.; Reese, M. O.; Ellingson, R. J.; Nozik, A. J. Schottky Solar Cells Based on Colloidal Nanocrystal Films. *Nano Lett.* **2008**, *8*, 3488–3492.
10. Johnston, K. W.; Pattantyus-Abraham, A. G.; Clifford, J. P.; Myrskog, S. H.; MacNeil, D. D.; Levina, L.; Sargent, E. H. Schottky-Quantum Dot Photovoltaics for Efficient Infrared Power Conversion. *Appl. Phys. Lett.* **2008**, *92*, 3.
11. Chuang, C.-H. M.; Brown, P. R.; Bulović, V.; Bawendi, M. G. Improved Performance and Stability in Quantum Dot Solar Cells through Band Alignment Engineering. *Nat. Mater.* **2014**, *13*, 796–801.
12. Ning, Z.; Voznyy, O.; Pan, J.; Hoogland, S.; Adinolfi, V.; Xu, J.; Li, M.; Kirmani, A. R.; Sun, J.-P.; Minor, J.; *et al*. Air-Stable n-Type Colloidal Quantum Dot Solids. *Nat. Mater.* **2014**, *13*, 822–828.
13. Xu, F.; Ma, X.; Haughn, C. R.; Benavides, J.; Doty, M. F.; Cloutier, S. G. Efficient Exciton Funneling in Cascaded PbS Quantum Dot Superstructures. *ACS Nano* **2011**, *5*, 9950–9957.
14. Wanger, D. D.; Correa, R. E.; Dauler, E. A.; Bawendi, M. G. The Dominant Role of Exciton Quenching in PbS Quantum-Dot-Based Photovoltaic Devices. *Nano Lett.* **2013**, *13*, 5907–5912.
15. Poulikakos, L. V.; Prins, F.; Tisdale, W. A. Transition from Thermodynamic to Kinetic-Limited Excitonic Energy Migration in Colloidal Quantum Dot Solids. *J. Phys. Chem. C* **2014**, *118*, 7894–7900.
16. Chappell, H. E.; Hughes, B. K.; Beard, M. C.; Nozik, A. J.; Johnson, J. C. Emission Quenching in PbSe Quantum Dot Arrays by Short-Term Air Exposure. *J. Phys. Chem. Lett.* **2011**, *2*, 889–893.
17. Gao, J. B.; Johnson, J. C. Charge Trapping in Bright and Dark States of Coupled PbS Quantum Dot Films. *ACS Nano* **2012**, *6*, 3292–3303.
18. Lingley, Z.; Lu, S. Y.; Madhukar, A. The Dynamics of Energy and Charge Transfer in Lead Sulfide Quantum Dot Solids. *J. Appl. Phys.* **2014**, *115*, 084302 .
19. Clark, S. W.; Harbold, J. M.; Wise, F. W. Resonant Energy Transfer in PbS Quantum Dots. *J. Phys. Chem. C* **2007**, *111*, 7302–7305.
20. Law, M.; Beard, M. C.; Choi, S.; Luther, J. M.; Hanna, M.; Nozik, A. J. Determining the Internal Quantum Efficiency of PbSe Nanocrystal Solar Cells with the Aid of an Optical Model. *Nano Lett.* **2008**, *8*, 3904–3910.
21. Noolandi, J.; Hong, K. M. Theory of Photogeneration and Fluorescence Quenching. *J. Chem. Phys.* **1979**, *70*, 3230–3236.
22. Leatherdale, C. A.; Kagan, C. R.; Morgan, N. Y.; Empedocles, S. A.; Kastner, M. A.; Bawendi, M. G. Photoconductivity in CdSe Quantum Dot Solids. *Phys. Rev. B* **2000**, *62*, 2669–2680.
23. Quintero-Torres, R.; van Veggel, F.; Young, J. F. Temperature Dependence of Forster Thermalization and Population

Decay in PbSe Nanocrystals. *J. Phys. Chem. C* **2014**, *118*, 1377–1385.
24. Zhang, J.; Tolentino, J.; Smith, E. R.; Zhang, J.; Nozik, A. J.; Beard, M. C.; Law, M.; Johnson, J. C. Carrier Transport in PbS and PbSe QD Films Measured by Photoluminescence Quenching. *J. Phys. Chem. C* **2014**, *118*, 16228–16235.
25. Chen, T.; Skinner, B.; Xie, W.; Shklovskii, B. I.; Kortshagen, U. R. Carrier Transport in Films of Alkyl-Ligand-Terminated Silicon Nanocrystals. *J. Phys. Chem. C* **2014**, *118*, 19580–19588.
26. Shklovskii, B. I.; Efros, A. L. *Electronic Properties of Doped Semiconductors*; Springer-Verlag: New York, 1984.
27. Liu, H.; Pourret, A.; Guyot-Sionnest, P. Mott and Efros-Shklovskii Variable Range Hopping in CdSe Quantum Dots Films. *ACS Nano* **2010**, *4*, 5211–5216.
28. Gonzalez-Rabade, A.; Morteani, A. C.; Friend, R. H. Correlation of Heterojunction Luminescence Quenching and Photocurrent in Polymer-Blend Photovoltaic Diodes. *Adv. Mater.* **2009**, *21*, 3924.
29. Tvingstedt, K.; Vandewal, K.; Zhang, F. L.; Inganas, O. On the Dissociation Efficiency of Charge Transfer Excitons and Frenkel Excitons in Organic Solar Cells: A Luminescence Quenching Study. *J. Phys. Chem. C* **2010**, *114*, 21824–21832.
30. Inal, S.; Schubert, M.; Sellinger, A.; Neher, D. The Relationship between the Electric Field-Induced Dissociation of Charge Transfer Excitons and the Photocurrent in Small Molecular/Polymeric Solar Cells. *J. Phys. Chem. Lett.* **2010**, *1*, 982–986.
31. Liu, Y.; Gibbs, M.; Puthussery, J.; Gaik, S.; Ihly, R.; Hillhouse, H. W.; Law, M. Dependence of Carrier Mobility on Nanocrystal Size and Ligand Length in PbSe Nanocrystal Solids. *Nano Lett.* **2010**, *10*, 1960–1969.
32. Erslev, P. T.; Chen, H.-Y.; Gao, J.; Beard, M. C.; Frank, A. J.; van de Lagemaat, J.; Johnson, J. C.; Luther, J. M. Sharp Exponential Band Tails in Highly Disordered Lead Sulfide Quantum Dot Arrays. *Phys. Rev. B* **2012**, *86*.
33. Mentzel, T. S.; Porter, V. J.; Geyer, S.; MacLean, K.; Bawendi, M. G.; Kastner, M. A. Charge Transport in PbSe Nanocrystal Arrays. *Phys. Rev. B* **2008**, *77*, 8.
34. Gao, J. B.; Luther, J. M.; Semonin, O. E.; Ellingson, R. J.; Nozik, A. J.; Beard, M. C. Quantum Dot Size Dependent J-V Characteristics in Heterojunction ZnO/PbS Quantum Dot Solar Cells. *Nano Lett.* **2011**, *11*, 1002–1008.
35. Leschkies, K. S.; Beatty, T. J.; Kang, M. S.; Norris, D. J.; Aydil, E. S. Solar Cells Based on Junctions between Colloidal PbSe Nanocrystals and Thin ZnO Films. *ACS Nano* **2009**, *3*, 3638–3648.